Biologically analogous calcium phosphate tubes from a chemical garden

Hughes, Erik; Williams, Richard; Cox, Sophie; Grover, Liam

DOI:
10.1021/acs.langmuir.6b04574

Document Version
Publisher's PDF, also known as Version of record

Citation for published version (Harvard):
Hughes, E, Williams, R, Cox, S & Grover, L 2017, 'Biologically analogous calcium phosphate tubes from a chemical garden', *Langmuir*, vol. 33, no. 8, pp. 2059-2067. https://doi.org/10.1021/acs.langmuir.6b04574

LANGMUIR

Article

pubs.acs.org/Langmuir

Biologically Analogous Calcium Phosphate Tubes from a Chemical Garden

Erik A. B. Hughes, Richard L. Williams, Sophie C. Cox, and Liam M. Grover*

School of Chemical Engineering, University of Birmingham, Edgbaston B15 2TT, U.K.

Supporting Information

ABSTRACT: Calcium phosphate ($CaPO_4$) tubes with features comparable to mineralized biological microstructures, such as Haversian canals, were grown from a calcium gel/phosphate solution chemical garden system. A significant difference in gel mass in response to high and low solute phosphate equivalent environments existed within 30 min of solution layering upon gel (p = 0.0067), suggesting that the nature of advective movement between gel and solution is dependent on the solution concentration. The transport of calcium cations (Ca^{2+}) and phosphate anions (PO_4^{3-}) was quantified and changes in pH were monitored to explain the preferential formation of tubes within a PO_4^{3-} concentration range of 0.5−1.25 M. Ingress from the anionic solution phase into the gel followed by the liberation of Ca^{2+} ions from the gel was found to be essential for acquiring self-assembled tubular $CaPO_4$ structures. Tube analysis by scanning electron microscopy (SEM), X-ray diffraction (XRD), and micro X-ray florescence (μ-XRF) revealed hydroxyapatite (HA, $Ca_{10}(PO_4)_6(OH)_2$) and dicalcium phosphate dihydrate (DCPD, $CaHPO_4{\cdot}2H_2O$) phases organized in a hierarchical manner. Notably, the tubule diameters ranged from 100 to 150 μm, an ideal size for the permeation of vasculature in biological hard tissue.

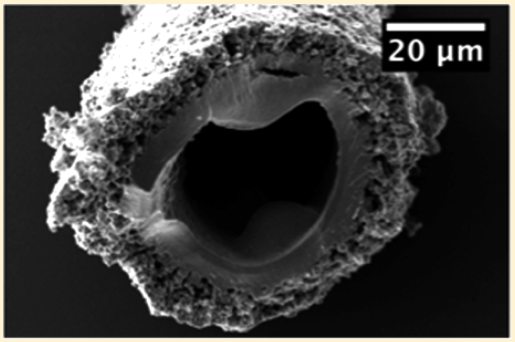

INTRODUCTION

Tubular mineralized structures that contribute to intricate arrangements and networks are found throughout nature, forming in bamboo, coccolithophores, corals, and exotic architectures such as the central rose of a water-pot shell.[1−7] Tubelike motifs are also found in the hard tissues of mammals, including dentinal tubules in teeth and Haversian canals in bone.[1−4] These features are not random, functioning to enable gases and nutrients to pass through tissues of relatively low pore volume and maintain the viability of embedded cell populations. Many presume that the formation of these tubes is entirely biologically driven by cellular processes.[8,9] Odontoblasts, for instance, are thought to play a significant role in guiding the formation of dentinal tubules.[10] Although often overlooked, physical processes, such as fluid flow, play a crucial role in the development of ear, kidney, and brain tissue.[11] A better understanding of these processes in terms of guiding mineral formations is desirable and may even assist in attempts to replicate hard tissue structure more closely for the purpose of advanced regenerative biomaterials. Disease processes may also be better understood. Osteophytes, for instance, are organized extrusions of mineral that extend from subchondral bone into the joint space and are pathological in osteoarthritis.[12]

A chemical garden commonly refers to solid elongated structures that form from the surface of a metal ion monolith when added to silicate solution.[13] Such systems remain of great interest to scientists since their conception in the early 17th century, having first been observed by German−Dutch alchemist Johann Glauber in 1646.[14] Fascination stems from their likeness to aforementioned mineralized structures that originate from both biotic and abiotic systems. Many combinations of reactive species can be combined in these systems, including but not limited to metallic cations of calcium (Ca^{2+}), strontium (Sr^{2+}), copper (Cu^{2+}), iron (Fe^{2+}), and cobalt (Co^{2+}) with anionic species of silicate (SiO_4^{4-}), carbonate (CO^{2-}), borate (BO_3^{3-}), and phosphate (PO_4^{3-}).[13−18] Complex osmotic processes drive the formation of these lifelike tubular precipitates, as understood through research predominantly undertaken in the 19th and 20th centuries.[14,19] Work by Kamiya et al. and more recently Steenbjerg Isben et al. disseminated the important mechanistic understanding of tubular architectures grown at a gel/solution interface, which form similarly to that of a chemical garden.[20,21] Formation begins when a semipermeable membrane is formed over the gel phase because of the initial reaction between cationic species in the gel and anions in the solution phase resulting in an insoluble reaction product. When osmotic forces allow, fluid rich in metal ions is liberated from the gel into the ionic solution phase, which self-assembles into hollow tubes whereby the gel pores serve as an initial template.[20,22] Continuous growth is confirmed to occur at the tips of already

Received: December 21, 2016
Revised: January 30, 2017
Published: January 30, 2017

DOI: 10.1021/acs.langmuir.6b04574
Langmuir 2017, 33, 2059−2067

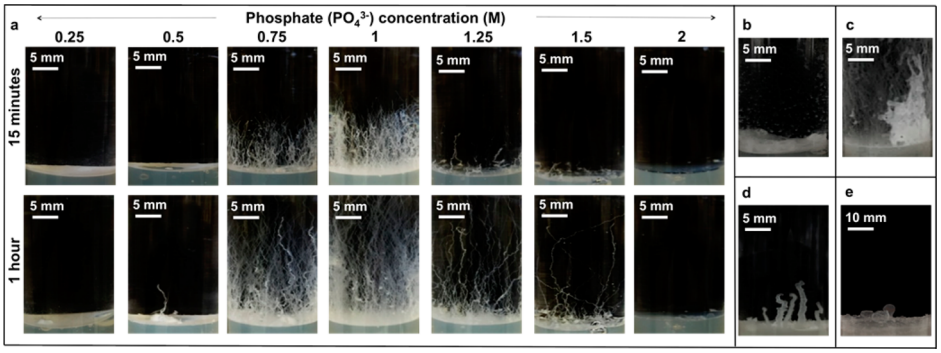

Figure 1. Influence of PO_4^{3-} concentration on $CaPO_4$ tube formation. Visualization of tube growth after 15 min and 1 h in 0.25−2 M PO_4^{3-} solutions (a), unstructured precipitate in 0.25 M PO_4^{3-} solution after 4 days (b), tube agglomeration and wall-bound growth in 1 M PO_4^{3-} solution after 4 days (c), thick budding tubes grown in 2 M PO_4^{3-} solution after 4 days (d), and sacklike morphologies grown in 2 M PO_4^{3-} solution after 4 days (e).

established tubes, maintained through repeating cyclic buildups of osmotic pressure and the release of cation-rich solution through a point of rupture. The necessary mass transport is facilitated by disequilibrium between species present on either side of the established semipermeable membrane.[18]

Despite this understanding, quantitative analysis surrounding chemical gardens remains unfortunately sparse.[23−25] Factors that determine tube growth rate are poorly understood but may be better explained through studying the rates of precipitation and advective transport,[26] providing complementary data to previous work on how precipitates form at gel/solution interfaces.[21] The gel/solution setup offers the opportunity for quantitative parameters to be measured that can be linked back to theoretical expectations of tube formation. In this article, the formation of tubules of calcium phosphate ($CaPO_4$) at the gel/solution interface was investigated. Solution movement in and out of a 1 M Ca^{2+} loaded agar gel was monitored in a PO_4^{3-}-rich environment, and the dependence of this exchange on tubule development by differing solute potential environments was investigated.

While osseous tissue scaffolds that are able to support the production of the bone extracellular matrix (ECM) have been developed, they suffer from poor vascularization.[27−29] $CaPO_4$ tubes, however, may possess a high surface area, narrow pore distribution, and mass transport viability,[30] offering enhanced cellular ingress and facilitation of directed angiogenesis and tubulogenesis for the generation of bony tissue in comparison to the current cohort of scaffold and unstructured calcium-based augmentation minerals.[29,31,32] Recent work regarding calcium silicate−phosphate tubes demonstrates the high potential of chemical garden structures to support the attachment and viability of mammalian cell cultures.[33] Microstructural and compositional characterization of $CaPO_4$ tubes was undertaken to assess their similarity to chemical garden structures, understand how they develop during formation, and assess their potential suitability to be explored further as an osteogenic self-assembling biomaterial.

EXPERIMENTAL METHOD

Calcium nitrate tetrahydrate ($Ca(NO_3)_2{\cdot}4H_2O$, 99%, ACS reagent), agar ($(C_{12}H_{18}O_9)_n$, for microbiology), ammonium phosphate dibasic ($(NH_4)_2HPO_4$, ≥98.0%, reagent grade), and sodium chloride (NaCl, ≥99%, ReagentPlus) were acquired from Sigma-Aldrich (U.K.). Distilled water was acquired from an arium advance EDI system. $Ca(NO_3)_2{\cdot}4H_2O$ was dissolved in 0.1 L of distilled water to a concentration of 1 M (or NaCl in the case of PO_4^{3-} in gel measurements to a concentration of 2 M), and 5 g of agar was added (with 250 μL of universal pH indicator (British Drug Houses Ltd., U.K.) for a selection of studies). The mixture was stirred at 250 rpm and heated to 80−90 °C on an MR Hei-Standard magnetic stirrer hot plate (Heidolph, Germany). After sufficient time to allow for the dissolution of the gel precursor, 2.5 mL of the gel mixture was siphoned into clear cylindrical containers. The mixture was given 24 h to complete gelation. $(NH_4)_2HPO_4$ (or NaCl for Ca^{2+} elution measurements) solutions were prepared as required, and 3 mL was layered over the set Ca^{2+} containing gel. pH was monitored using a calibrated S220 Seven Compact pH/ion meter equipped with an InLab Expert Pro pH probe (Mettler Toledo, USA).

The Supporting Information (SI) contains a detailed account of the methodologies for gel mass gain/loss (Figure S1a,b), the elution of Ca^{2+} from the gel phase into the solution phase (Figure S2 and eq S1), the ingress of PO_4^{3-} into the gel from the solution phase (Figure S3 and eq S2), scanning electron microscopy (SEM), X-ray diffraction (XRD), and micro X-ray fluorescence (μ-XRF).

RESULTS AND DISCUSSION

Initial Observations and Understanding $CaPO_4$ Chemical Garden Growth Regimes. Nodular and unstructured $CaPO_4$ precipitate was observed at the gel/solution interface in PO_4^{3-} solutions of between 0.25 and 0.5 M (Figure 1a,b). Generally, solutions between 0.5 and 1.5 M PO_4^{3-} resulted in substantially faster rates of tube formation and a larger number (75−125 tubules per 236 mm^2) (Figure 1a). The macromorphology of these tubes is typically straight with kinks, suggesting a jetting and popping regime of growth. Different growth regimes occur as a consequence of variations in the anionic solution density. Low-density Ca^{2+} solution entering the PO_4^{3-} solution phase can either rise quickly to produce a jet that catches to form a straight tube section or lead to oscillatory tube growth characterized by budding architectures and alterations in tube growth direction.[15] The tube length was observed to reach several centimeters within 15 min, and within 2 h it appeared that some tubes had begun to agglomerate because of a lack of free growth space that resulted in wall-bound features after several days (Figure 1c).

Initially, the layering of 2 M PO_4^{3-} solutions upon the gel phase produces no $CaPO_4$ precipitate. On occasion, relatively thick tubes were observed in 2 M PO_4^{3-} solutions after a few days (Figure 1d). These tubes were evidently wider than those grown in 0.5−1.5 M PO_4^{3-} solutions and were synonymous with a budding regime of tube growth, forming from the release of less buoyant cationic solution providing a wider tube girth at the origin of growth.[13−16] Similarly thick tubes that formed in a

DOI: 10.1021/acs.langmuir.6b04574
Langmuir 2017, 33, 2059−2067

chemical garden consisting of a calcium chloride ($CaCl_2$) seed in 6 M silicate solution have been reported.[15] It is suggested that air bubbles developed in the concentrated (6 M) and viscous silicate solutions used, acting as templates for wide tubes at the origin of growth.[15] Although air bubbles were not observed to aid the formation of $CaPO_4$ structures, they provide an interesting means for controlling tube growth parameters that has been explored elsewhere.[34,35] As well as thick tubes, $CaPO_4$ sacklike morphologies arose in some 2 M PO_4^{3-} solutions, which likely formed through the inflation of the precipitate membrane with Ca^{2+}-rich liquid without sufficient osmotic force to cause rupture (Figure 1e).

The growth behavior and resulting morphology of tubules among thin shoots of material, thicker tubules, and inflated sacks is partially linked to the development of a semipermeable precipitate membrane upon the gel/solution interface due to the reaction between metal ions and reactive anions in solution. For the analogous classical setup, it is believed that concentrated anionic solutions produce a firmer colloidal membrane that is more difficult to rupture, promoting membrane inflation, whereas relatively lower concentrations produce a comparably weaker membrane that can be more easily penetrated by metal ion streams to go to form tubes.[13−16] Similar tube morphology and growth characteristics are observed for $CaPO_4$ tubes grown in low (0.25 M) and high (2 M) PO_4^{3-} solution concentrations (Figure 1a). The growth mechanism that results in $CaPO_4$ morphologies is further discussed in this work alongside the fundamental experimental data.

When PO_4^{3-} solutions were layered upon the Ca^{2+} gel phase, a concentration-dependent coverage of precipitation was observed. Between 0.25 and 0.5 M PO_4^{3-}, a membrane of precipitate formed that occupied 99.6 and 63% of the gel/solution interface, respectively (Figure 2). At 0.25 M PO_4^{3-}, membrane rupture results in jetting streams of $CaPO_4$ material that fail to form tubes, consistent with the proposition of a weak rupture membrane.[13−16] In relatively low concentrations of PO_4^{3-} solutions (0.25−0.5 M), the $CaPO_4$ membrane may take longer to form, as the initial precipitate membrane disappears within 2 h and tubes are visible only after this time. For PO_4^{3-} solutions in the concentration range between 0.75 and 1.25 M, localized spots of precipitate were visible on the gel solution interface, which provided the origin of tubes that formed immediately. Despite the expectation of a precipitate membrane when solutions of 2 M PO_4^{3-} were employed, no precipitate coverage was observed on the gel/solution surface. It is possible that the required levels of Ca^{2+} and PO_4^{3-} ions are insufficient to induce precipitation when 2 M PO_4^{3-} is immediately layered upon gel. Alternatively, the ionic concentration of both species may well be sufficient for precipitation; however, the increased concentration of non-precipitate counterions may decrease the effective concentration of Ca^{2+} and PO_4^{3-} in solution through ionic shielding phenomena.[36] Ionic shielding involves counterions surrounding reactant ions of opposite change in solution, preventing them from reacting even in concentrated solutions where products would be expected to form.[36] An extended induction time is evidently required for the precipitate reaction of Ca^{2+} and PO_4^{3-} ions in these systems, eventually resulting in structures (Figure 1d,e). The inflated nature of constructs that are produced suggests that despite taking longer to develop, the resulting membrane can resist rupture to an extent beyond that formed in solutions <2 M. However, whereas optimum solution concentration ranges for inducing tubules have been explored in different chemical garden systems, the observation and quantification of a concentration-dependent precipitate coverage of the cationic source, in this case the Ca^{2+}-loaded gel, have not previously been reported for chemical garden systems. The color similarity between the newly forming precipitate and the crystal seed makes this differentiation difficult in the classical setup. Hence, the use of a gel/solution system may enable us to gather further mechanistic insights into tube-formation within chemical gardens.

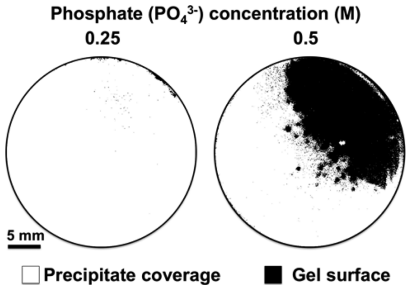

Figure 2. Top-down view of the binary image of the typical $CaPO_4$ precipitation coverage formed on the gel/solution interface for PO_4^{3-} solutions of 0.25 and 0.5 M 1 min after layering on the gel surface.

Response of the Gel Phase to Varying Solute Potential. Gel mass change experiments were conducted in solutions of 1 and 5 M NaCl as opposed to PO_4^{3-} in order to avoid initiating precipitation; selected solutions exhibit an equivalent solute potential to PO_4^{3-} solutions of 0.5 and 2.5 M, respectively, calculated using the van't Hoff equation (eq S3 and Table S1). Gel mass gain/loss profiles were dynamic in both 1 and 5 M NaCl solutions (Figure 3). As expected, a 1 M NaCl solution brought about an initial gradual gel mass increase in the first 3 min (+2.7 ± 0.2%), measured at its most substantial value after 10 min (+3.2 ± 1.6%), because of the potential gradient favoring the net movement of solution into the gel from the solution phase. Gels in 5 M NaCl solutions decreased in mass by 0.7 ± 0.3% after 10 min because of the potential gradient favoring the net movement of Ca^{2+}-rich solution out of the gel into the solution phase (Figure 3). At 30 min, despite gaining some mass, the gels in 5 M PO_4^{3-} solution remained in a net mass loss regime (−0.1 ± 0.5%) before further mass decrease at 2 h (−1.4 ± 1.7%). Statistical analysis

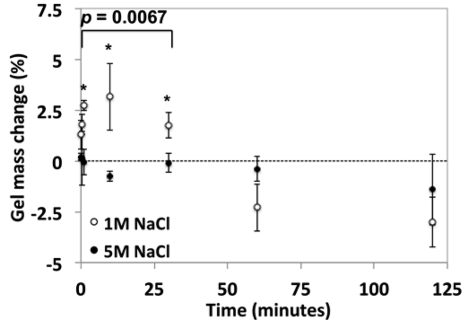

Figure 3. Mass gain/loss profile of gels exposed to 1 and 5 M NaCl solutions between 0 and 120 min (error bars represent the standard deviation for n = 3 measurements of individual samples, * = significance as determined by post hoc t test analysis, where p = <0.05).

DOI: 10.1021/acs.langmuir.6b04574
Langmuir 2017, 33, 2059−2067

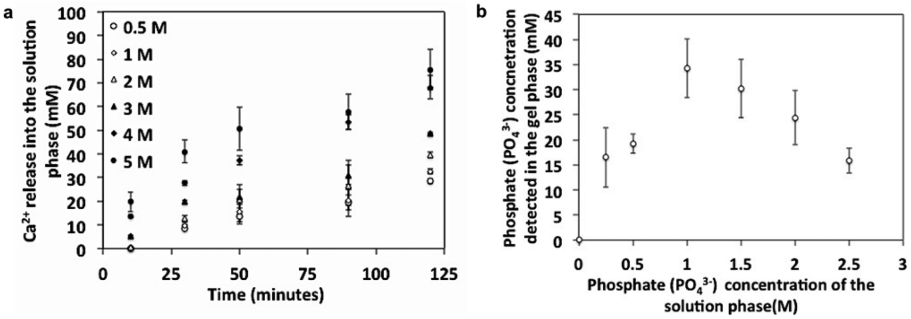

Figure 4. Ca^{2+} release into bulk solution as a function of the NaCl solution concentration (error bars represent the standard deviation for $n = 3$ measurements of individual samples) (a) and PO_4^{3-} ingress into the gel as a function of the PO_4^{3-} solution concentration (error bars represent the standard deviation for $n = 2$ measurements of individual samples) (b).

performed using two-way ANOVA revealed a significant difference in the gel mass gain/loss response from the employment of low concentration (1 M NaCl) and high concentration (5 M NaCl) solution environments (F (1, 4) = 26.57, p = 0.0067) within the first 30 min of gel exposure to solution. Post hoc t tests revealed the significance among the mass gain/loss gel responses at 1 min (p = 0.0067), 3 min (p = 0.037), and 10 min (p = 0.012).

These results go some way to understanding the preferential formation of $CaPO_4$ tubes in PO_4^{3-} solutions between 0.5 and 1.5 M. Between these concentrations, osmotic driving forces appear to drive the movement of solution across the semipermeable precipitate barrier, with the coverage taking the form of a sheet or localized spots on the gel/solution interface, toward the gel. Consequently, the gel mass increase leads to a buildup in osmotic pressure. To counteract this, the pressure is relieved through rupturing the precipitate membrane, which releases streams of Ca^{2+}-rich solution into the corresponding solution of PO_4^{3-}. The jetting and occasional oscillatory nature of these Ca^{2+} streams provide a template for the growth of tubular constructs with straight and kinked macromorphology (Figure 1a). Solutions of PO_4^{3-} on either side of the 0.5−1.5 M concentration range as investigated through NaCl solutions with matching solute potentials appear not to elicit a gel mass increase but rather a decrease indicating that solution is expelled. As such, the buildup of osmotic pressure within the gel does not take place, and tubes are not immediately formed from the employment of PO_4^{3-} solutions of 0.25 and 2 M.

Ca^{2+} and PO_4^{3-} Ion Transport. The release of Ca^{2+} ions occurred in all NaCl solutions in the range of 0.5−5 M and progressed steadily with time (Figure 4a). Expectedly, the elution rate increased gradually with increasing NaCl solution concentration because the potential for ionic Ca^{2+} movement from gel into solution phase proportionally intensifies in more concentrated solution environments.

Before layering with PO_4^{3-}solutions, the PO_4^{3-} concentration found in the gel existed at a comparatively low concentration of 0.11 ± 0.00 mM (Figure 4b). After 30 min, the concentration of PO_4^{3-} in the gel peaked at 34.30 ± 5.87 mM when the PO_4^{3-} concentration of the solution was 1 M and decreased at higher PO_4^{3-} concentrations in the solution phase; the ingress of PO_4^{3-} into the gel as a function of the initial PO_4^{3-}concentration in solution was therefore not monotonic and did not follow the same trend as Ca^{2+} release into the anionic solution phase (Figure 4b).

Observing pH Change as an Indicator of Ionic Movement. A capillary tube was inserted just below the gel/solution interface allowing the collection of ejected calcium-rich solution from the gel (Figure 5a). A universal pH indicator

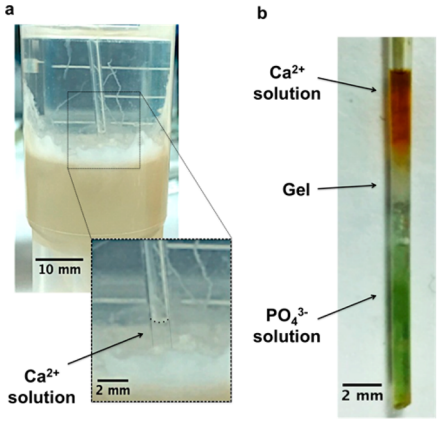

Figure 5. Ca^{2+}-rich solution as collected in a capillary tube placed at the gel/solution interface (a), followed by the removal of the capillary tube and staining of the collected contents with universal pH indicator (b) (PO_4^{3-} solution was drawn up the capillary tube on pull out).

revealed the acidic nature of the Ca^{2+}-rich fluid in contrast to the neutral-alkali nature of the PO_4^{3-} solution that had also been collected on pull out (Figure 5b and s4). The pH of the gel mixture before heating and setting was determined to be 4.5−5.5, and gels stained with universal pH indicator became orange as a result of the acidic cationic environment. The PO_4^{3-} solution pH was between 8 and 9.

$CaPO_4$ tubes form preferentially in regions where the pH at the gel/solution interface experiences a substantial shift to alkalinity by turning blue or purple in the gel phase (Figures 6a and S4, Movie S1). Regions that did not experience this shift resulted in little or poor $CaPO_4$ tubular growth but sometimes developed a red coloration band at the gel/solution interface (Figure 6a, Movie S1). Similar experiments have shown that although shifts in pH are not a trigger for tubule formation but rather a byproduct of precipitate development, measurements of pH can be utilized as an indicator of solution exchange and tubule formation.[21]

The layering of 0.25 and 0.5 M PO_4^{3-} solutions facilitated a red (acidic) band at the gel/solution interface (Figure 6b) that was more prominent in gels layered with 0.25 M solutions (Figure 6c). From Ca^{2+} release measurements (Figure 3a), the release of Ca^{2+} ions was less extensive in equivalent 0.25 M

DOI: 10.1021/acs.langmuir.6b04574
Langmuir 2017, 33, 2059−2067

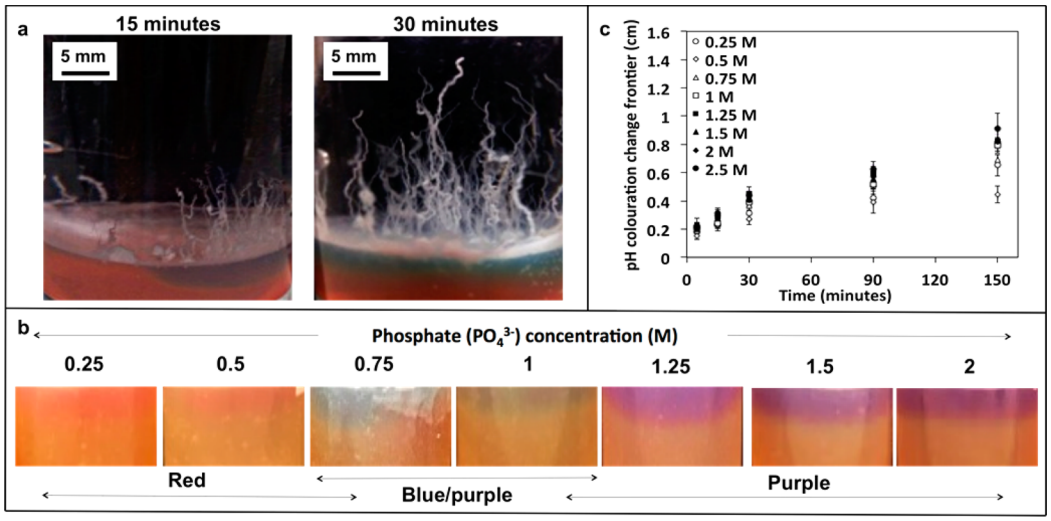

Figure 6. Universal pH indicator stained gel layered with 0.5 M PO_4^{3-} solution changing coloration in response to $CaPO_4$ tubular formation (a). Gels stained with universal pH indicator and layered with 0.25−5 M PO_4^{3-} solutions (field of view ∼30 mm) (b) and quantification of the coloration band depth (error bars represent the standard deviation for n = 3 measurements of individual samples) (c).

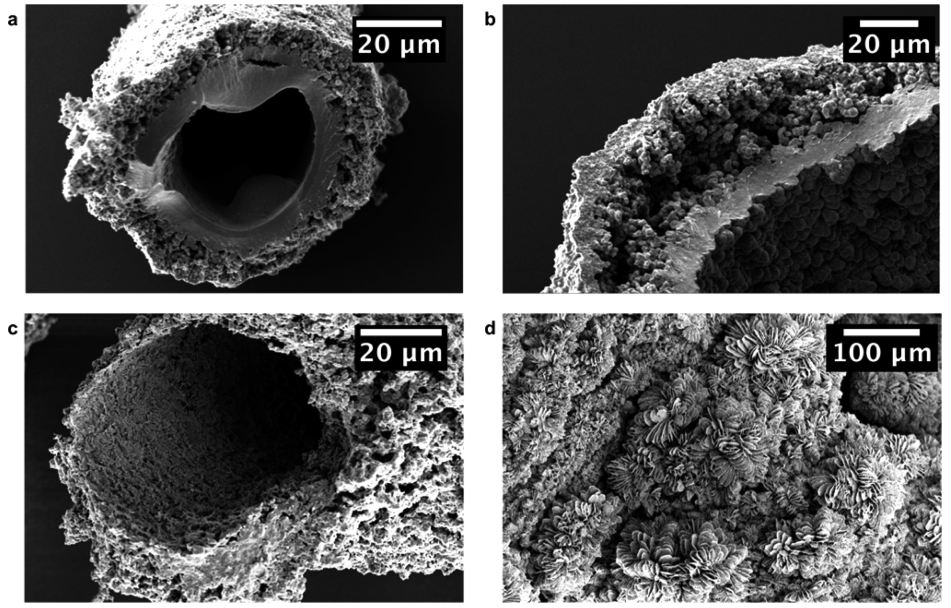

Figure 7. Micrographs of $CaPO_4$ tubes grown in 0.5 M PO_4^{3-} solutions extracted at 5 h (a) and 24 h (b), $CaPO_4$ tubes grown in 1.25 M PO_4^{3-} solutions (c), and $CaPO_4$ tubes grown in 2 M PO_4^{3-} solutions (d) extracted at 10 days.

PO_4^{3-} solutions than in 0.5 M PO_4^{3-} solutions. Therefore, red coloration represents a buildup of unreleased acidic Ca^{2+} ions just below the gel/solution interface, which ultimately delays the onset of tubules (Figure 1a). Red (acidic) banding eventually turned blue (increasingly alkaline) when both 0.25 and 0.5 M PO_4^{3-} solutions were used and coincided with the onset of the $CaPO_4$ nodular precipitate and tubular structure formation, respectively (Figures 1a and 6a). Coloration at the gel/solution interface for gels layered with 0.75 and 1 M PO_4^{3-} solutions was blue (alkali) initially before appearing purple (stronger alkali). Gels layered with solutions of between 1.25 and 2.5 M PO_4^{3-} developed a purple band immediately. The depth of the alkaline coloration bands increased with increasing PO_4^{3-} solution concentration in the range of 0.75−2 M (Figure 6b,c), which correlates to the exodus of Ca^{2+} ions and ingress of PO_4^{3-} anions into the gel by solution movement (Figures 3 and 4a,b). The resulting exchange of ions promotes the induction of tubule formation above the gel/solution interface in 0.75−1.5 M PO_4^{3-} solutions (Figure 1a). This does not necessarily correlate with the formation of precipitate in 2 M PO_4^{3-} solutions. A relatively high concentration of Ca^{2+} ions released into 2 M PO_4^{3-} solution suggests that supersaturation criteria for $CaPO_4$ precipitation are met (Figure 4a), and previously alluded to ionic shielding effects ultimately diminish the effective concentration of ions available to react.[36]

Microstructural and Compositional Evolution of $CaPO_4$ Tubes. A tube-widening phenomenon was observed from micrographs of $CaPO_4$ tubes grown in 0.5 M PO_4^{3-} solutions over 24 h. Tubes typically matured to a final diameter of 100−150 μm and possessed a bilayer wall consisting of a porous outer layer (∼10 μm) and continuous inner layer (∼10 μm) that is consistent with the microstructure of chemical gardens[18] (Figure 7a). This arrangement is comparable to the structuring of micrometer-width dentinal tubules, although

DOI: 10.1021/acs.langmuir.6b04574
Langmuir 2017, 33, 2059−2067

existing at length scales typical of Haversian canals that at maturity exhibit an average diameter of between 50 and 200 μm in human bone.[1,4,9,37,38]

At 24 h, widened tubes possessed a diameter of >300 μm, and a gap space developed between the outer and inner tube layers, suggesting immiscible phase separation (Figure 7b). A close inspection of the walls of typical and widened tubes revealed that both the inner and outer thicknesses remained ~10 μm per layer. The wall thickness may be maintained through a spontaneous self-healing mechanism that allows for total tube widening while maintaining the thickness of the tube walls in order to support structural integrity and microstructural evolution.[14] In response to increased periods of cationic fluid flow that are dependent on solution potential differences between cationic and anionic phases, tubes may expand.

The diameter of $CaPO_4$ tubes from PO_4^{3-} solutions between 0.75 and 1.5 M ranged from 100 to 150 μm (Figure 7c). Tubes grown in 0.75 and 1 M PO_4^{3-} solutions had a microstructure similar to those grown in 0.5 M PO_4^{3-}, possessing a porous outer layer and a continuous inner layer. In contrast, tubes grown in 1.25 and 1.5 M PO_4^{3-} solutions possessed a single porous wall that was microstructurally similar to the outer wall of tubes that exhibited a bilayer structure (Figure 7c). Tubes grown in 2 M PO_4^{3-} had a strikingly different microstructure that consisted of organized flowering flake clusters (Figure 7d). The diameter of these tubes was also considerably wider (500–600 μm).

It is evident that the scale and microstructure of these tubes mimic intrinsic features of natural bone tissue at the length scale of Haversian canals that house vascular networks. As such, the fabrication of $CaPO_4$ tubules may be of interest for replicating these structures through physical phenomena at gel/solution interfaces.

X-ray diffraction patterns were collected to study the evolution of crystallinity and the crystalline phase during initial precipitate formation in 0.5 M PO_4^{3-} solutions (Figure 8a). After 3 and 5 h, the precipitate consisted of poorly crystalline apatite, as suggested by the broad peaks, which correlate well with the diffraction pattern of hydroxyapatite (HA, $Ca_{10}(PO_4)_6(OH)_2$, ICDD-01-074-9761). After 24 h, peaks matching dicalcium phosphate dihydrate (DCPD, $CaHPO_4 \cdot 2H_2O$, ICDD-04-013-3344) were detected, which became noticeably more pronounced and sharper with increasing time.

The crystalline composition of tubes grown in PO_4^{3-} solutions of 0.25–1.5 M was also assessed after 30 days of aging (Figure 8b). Peaks corresponding to both HA and DCPD were still present in the diffraction pattern of the 0.5 M PO_4^{3-} precipitate (Figure 8b). Patterns collected for all other solution concentrations also matched the HA and DCPD references (Figure 8c). The phase composition of similarly prepared $CaPO_4$ tubes was previously determined to consist of a mixture of HA and DCPD phases.[20,22] The resulting $CaPO_4$ phase is highly dependent on the solution environment, with prominent factors, including pH and solubility, influencing the formation of minerals. Both of these phases are of biological importance within mammalian systems. For instance, HA is the primary mineral component of hard tissue and provides a physiological stable phase that can support the growth and proliferation of osteogenic bone-forming cells.[1,27]

The presence of highly soluble phases was also detected: biphosphammite ($NH_4H_2PO_4$, ICDD-01-072-4581) in precipitates grown in 0.75 and 1.5 M PO_4^{3-} solutions and nitrammite (NH_4NO_3, ICDD-00-047-0867) found in precipitates grown in

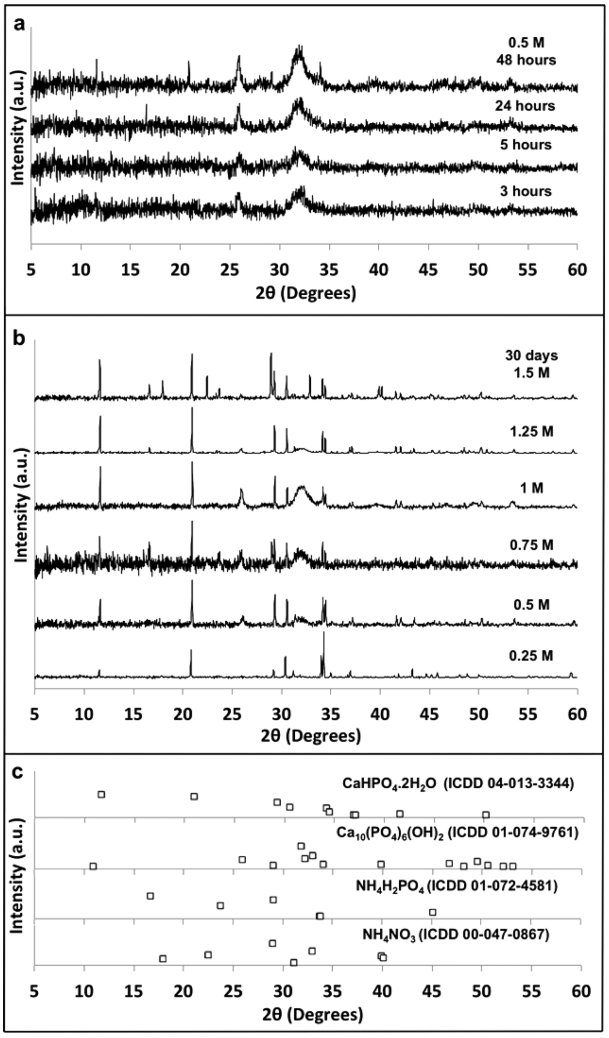

Figure 8. XRD diffraction patterns of the development of $CaPO_4$ precipitate grown for up to 48 h in PO_4^{3-} 0.5 M solutions (a) and after 30 days for $CaPO_4$ precipitates grown in 0.25–1.5 M PO_4^{3-} solutions (b). ICDD reference patterns for $CaHPO_4 \cdot 2H_2O$, $Ca_{10}(PO_4)_6(OH)_2$, $NH_4H_2PO_4$, and NH_4NO_3 matched collected patterns (c).

1.5 M PO_4^{3-} solutions (Figure 8b,c). The reagent salts employed in tube-formation experiments provide ions required to produce such phases, which have not been fully washed away after precipitate extraction.

$CaPO_4$ tube structures are compositionally heterogeneous in nature during growth: a growing acidic Ca^{2+}-rich core that evolves through an alkali PO_4^{3-} solution phase. Bilayer tube wall formation, best observed in micrographs of $CaPO_4$ tubes grown in 0.5 M PO_4^{3-} solution after 5 and 24 h (Figure 7a,b), can therefore be explained. An amorphous outer wall of the $CaPO_4$ tubes is likely to comprise a low-crystallinity HA precipitate that is the first to develop, before the formation of an inner wall composed of DCPD because XRD patterns show that amorphous HA phase development precedes that of DCPD while also being consistent with the fact that chemical garden tube wall thickness develops inward via propagating reaction-diffusion front and the pH profile.[18] Similar to the synthesis of mineral phases in many organisms, self-assembling $CaPO_4$ tubes evidently exhibit exceptional thermodynamic and kinetic control of precipitating amorphous and crystalline mineral phases.[39] As such, the employment of a gel/solution

DOI: 10.1021/acs.langmuir.6b04574
Langmuir 2017, 33, 2059–2067

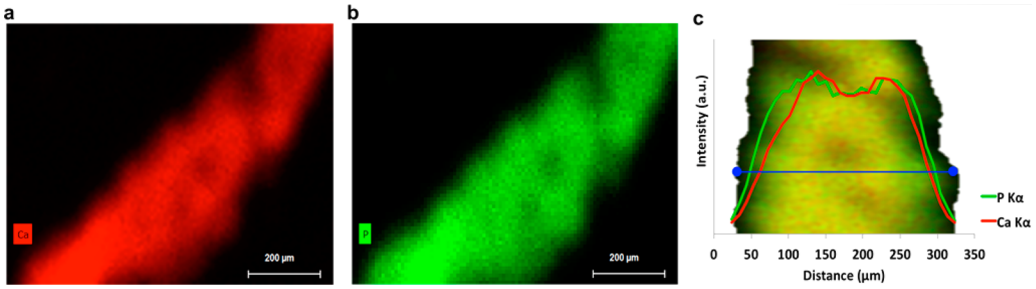

Figure 9. μ-XRF maps of a $CaPO_4$ tube structure grown in 0.5 M PO_4^{3-} solution. Elemental mapping of calcium (a) and phosphorus (b). Elemental maps of calcium and phosphorus were combined; the calcium and phosphorus Kα signal intensities of both elements were plotted from a line scan (blue) taken along the tube circumference (c).

model for creating structured mineral far surpasses many synthetic mineral synthesis pathways associated with combining ionic solutions that result in the precipitation of mineral crystals.

Elemental analysis was undertaken on tubes grown in 0.5 M PO_4^{3-} solutions to further understand the tube wall composition using a μ-XRF mapping instrument. The scanning area was selected in order to reveal the chemical composition along the tube length. The major elemental components of the tubes were calcium and phosphorus distinguished by Kα lines appearing in the expected vicinity of 3.69 and 2.01 keV, respectively, and an additional line for Ca (Kβ at 4.01 keV) was also observed (Figure S5). Mapping of the additional elements detected, namely, aluminum (Al), silicon (Si), sulfur (S), chlorine (Cl), potassium (K), iron (Fe), and copper (Cu) showed these elements to reside outside of the tube structure, originating from the background material upon which the tubule sample is supported.

Elemental maps of calcium (Figure 9a) and phosphorus (Figure 9b) were combined, and a line scan was collected across the diameter of the tube (Figure 9e). This allowed the Ca and P signal intensities to be plotted along the selected line scan. The outer tube wall was found to be relatively P-rich (Figure 9c), which supports the proposed compositional hierarchy of an HA outer layer that develops into a DCPD inner layer. This biphasic ordering of compositional phases is obtained through the exposure of the developing precipitate to an acidic Ca^{2+}-rich core and an alkaline PO_4^{3-} exterior, shedding light on how the creation of similar structures may be obtained from physical driving forces that are currently possible only in biological systems.

Acquiring control of these structuring processes may allow for designer $CaPO_4$ regenerative biomaterials. Desirable features include similar composition and architecture to naturally occurring dentinal tubules and Haversian canals capable of directing angiogenesis and tubulogenisis processes beyond synthetic systems through the provision of high surface area, porosity, and mass transport facilitation.[28−32] Promisingly, mineral tubular constructs can support the viability of cell cultures, and further ways in which to incorporate biological cells during tube fabrication are active areas of research, bridging the gap between chemical gardens and tissue engineering applications.[33,40]

CONCLUSIONS

Long-standing interest in chemical garden structures goes back as far as the 17th century and stems from their resemblance to a number of naturally occurring formations such as hydrothermal vents on the sea floor and mineralized biological structures such as corals, shells, and mammalian bone. Here we generate $CaPO_4$ tubules that resemble dentinal tubules and Haversian canals found in human hard tissues. This supports the notion that not only biological processes but also physical driving forces play a fundamental role in biotic structuring.

Compiling results associated with the mechanism of $CaPO_4$ precipitation and tubular formation in a gel/solution setup, it is evident there is a complex relationship between Ca^{2+} gel and PO_4^{3-} solution phases that allows for the formation of chemical garden structures. $CaPO_4$ tube morphology was initiated only by specific PO_4^{3-} solutions in a range of 0.5−1.5 M. A significant difference was found in the gel response to either high or low solute environments of 1 and 5 M NaCl solutions, respectively, within 30 min. Conditions that facilitate the self-assembly of $CaPO_4$ tubular structures are an increase in gel mass followed by a decrease, representative of an influx of solution into the gel driven by osmotic forces and the subsequent release of Ca^{2+} -rich fluid to relieve osmotic pressure, as supported by gel Ca^{2+} release and PO_4^{3-} ingress measurements. Although gels layered with 2 M experience a substantial exodus of Ca^{2+} as determined by direct measurement and observation of a gel pH change, $CaPO_4$ precipitate and tube formation are likely initially inhibited by ionic shielding.

The presence of contrasting pH environments, namely, an acidic Ca^{2+}-rich fluid traveling through $CaPO_4$ tube structures and alkali PO_4^{3-} ion solution external to $CaPO_4$ tubes, drives the development of differing crystalline phases that constitute the hierarchical tube microstructure. Typical $CaPO_4$ tubes possessed a bilayer structure composed of an outer layer of HA and an inner layer of DCPD. Mastering control of the generation of these structures may allow the creation of regenerative biomaterials that are comparable to human tissue architecture and composition.

ASSOCIATED CONTENT

Supporting Information

The Supporting Information is available free of charge on the ACS Publications website at DOI: 10.1021/acs.langmuir.6b04574.

Detailed experimental methods and figures (PDF)

Relationship between the growth of $CaPO_4$ tubes and the change in pH at the gel/solution interface (ZIP)

AUTHOR INFORMATION

Corresponding Author

*E-mail: l.m.grover@bham.ac.uk.

DOI: 10.1021/acs.langmuir.6b04574
Langmuir 2017, 33, 2059−2067

ORCID

Erik A. B. Hughes: 0000-0003-2850-721X

Notes

The authors declare no competing financial interest.

■ ACKNOWLEDGMENTS

We acknowledge the EPSRC for funding this project (1294393 - medical materials) in association with TWI Ltd. SEM was undertaken with the help of Jianguo Liu in the School of Dentistry at the University of Birmingham. XRD and Raman spectroscopy were performed at the Advanced Materials Facility in the School of Chemistry at the University of Birmingham with the help of Jackie Deans.

■ REFERENCES

(1) Wegst, U. G. K.; Bai, H.; Saiz, E.; Tomsia, A. P.; Ritchie, R. O. Bioinspired structural materials. *Nat. Mater.* **2014**, *14* (1), 23−36.

(2) Pazzaglia, U. E.; Congiu, T.; Raspanti, M.; Ranchetti, F.; Quacci, D. Anatomy of the Intracortical Canal System: Scanning Electron Microscopy Study in Rabbit Femur. *Clin. Orthop. Relat. Res.* **2009**, *467*, 2446−2456.

(3) Enderle, J. D.; Bronzino, J. D. *Introduction to Biomedical Engineering*; Academic Press, 2012.

(4) Earl, J. S.; Leary, R. K.; Perrin, J. S.; Brydson, R.; Harrington, J. P.; Markowitz, K.; Milne, S. J. Characterization of dentine structure in three dimensions using FIB-SEM. *J. Microsc.* **2010**, *240* (1), 1−5.

(5) Marsh, M. E. Regulation of $CaCO_3$ Formation in Coccolithophores. *Comp. Biochem. Physiol., Part B: Biochem. Mol. Biol.* **2003**, *136* (4), 743−754.

(6) Liu, P.-J. Burrow Architecture of the Spionid Polychaete Polydora villosa in the Corals Montipora and Porites. *Zool. Stud.* **2000**, *39* (1), 47−54.

(7) Cardoso, S. S.; Cartwright, J. H. E.; Checa, A. G.; Sainz-Díaz, C. I. Fluid-flow-templated self-assembly of calcium carbonate tubes in the laboratory and in biomineralization: The tubules of the watering-pot shells, Clavagelloidea. *Acta Biomater.* **2016**, *43*, 338−347.

(8) Frost, H. M. *Bone Remodelling Dynamics*; Thomas: Springfield, IL, 1963.

(9) Maggiano, I. S.; Maggiano, C. M.; Clement, J. G.; Thomas, C. D. L.; Carter, Y.; Cooper, D. M. L. Three-dimensional reconstruction of Haversian systems in human cortical bone using synchrotron radiation-based micro-CT: morphology and quantification of branching and transverse connections across age. *J. Anat.* **2016**, *228* (5), 719−732.

(10) Arana-Chavez, V. E.; Massa, L. F. Odontoblasts: the cells forming and maintaining dentine. *Int. J. Biochem. Cell Biol.* **2004**, *36* (8), 1367−1373.

(11) Cartwright, J. H. E.; Piro, O.; Tuval, I. Fluid dynamics in developmental biology: moving fluids that shape ontogeny. *HFSP J.* **2009**, *3* (2), 77−93.

(12) van der Kraan, P. M.; van den Berg, W. B. Osteophytes: relevance and biology. *Osteoarthr. Cartil.* **2007**, *15* (3), 237−244.

(13) Cartwright, J. H.; Garcia-Ruiz, J. M.; Novella, M. L.; Otalora, F. J. Formation of Chemical Gardens. *J. Colloid Interface Sci.* **2002**, *256*, 351−359.

(14) Barge, L. M.; Cardoso, S. S.; Cartwright, J. H.; Cooper, G. J.; Cronin, L.; De Wit, A.; Doloboff, I. J.; Escribano, B.; Goldstein, R. E.; Haudin, F.; Jones, D. E.; Mackay, A. L.; Maselko, J.; Pagano, J. J.; Pantaleone, J.; Russell, M. J.; Sainz-Diaz, C. I.; Steinbock, O.; Stone, D. A.; Tanimoto, Y.; Thomas, N. L. From Chemical Gardens to Chemobrionics. *Chem. Rev.* **2015**, *115* (16), 8652−8703.

(15) Cartwright, J. H.; Escribano, B.; Sainz-Daz, C. I. Chemical-garden formation, morphology, and composition. I. Effect of the nature of the cations. *Langmuir* **2011**, *27* (7), 3286−3293.

(16) Coatman, R. D.; Thomas, N. L.; Double, D. D. Studies of the growth of "silicate gardens" and related phenomena. *J. Mater. Sci.* **1980**, *15*, 2017−2026.

(17) Barge, L. M.; Doloboff, I. J.; White, L. M.; Stucky, G. D.; Russell, M. J.; Kanik, I. Characterization of iron-phosphate-silicate chemical garden structures. *Langmuir* **2012**, *28* (8), 3714−3721.

(18) Steinbock, O.; Cartwright, J. H. E.; Barge, L. M. The fertile physics of chemical gardens. *Phys. Today* **2016**, *69* (3), 44−51.

(19) Hazlehurst, T. H. Structural Precipitates: The Silicate Garden Type. *J. Chem. Educ.* **1941**, *18*, 286−289.

(20) Kamiya, K.; Yoko, T.; Tanaka, K.; Fujiyama, Y. Growth of fibrous hydroxyapatite in the gel system. *J. Mater. Sci.* **1989**, *24* (3), 827−832.

(21) Steenbjerg Ibsen, C. J.; Mikladal, B. F.; Bjornholt Jensen, U.; Birkedal, H. Hierarchical tubular structures grown from the gel/liquid interface. *Chem. - Eur. J.* **2014**, *20* (49), 16112−16120.

(22) Tanahashi, M.; Kamiya, K.; Suzuki, T.; Nasu, H. Fibrous hydroxyapatite grown in the gel system: effects of pH of the solution on the growth rate and morphology. *J. Mater. Sci.: Mater. Med.* **1992**, *3* (1), 48−53.

(23) Haudin, F.; Cartwright, J. H.; Brau, F.; De Wit, A. Spiral precipitation patterns in confined chemical gardens. *Proc. Natl. Acad. Sci. U. S. A.* **2014**, *111* (49), 17363−17367.

(24) Thouvenel-Romans, S.; van Saarloos, W.; Steinbock, O. Silica tubes in chemical gardens: Radius selection and its hydrodynamic origin. *Europhys. Lett.* **2004**, *67* (1), 42−48.

(25) Roszol, L.; Steinbock, O. Controlling the wall thickness and composition of hollow precipitation tubes. *Phys. Chem. Chem. Phys.* **2011**, *13* (45), 20100−20103.

(26) Batista, B. C.; Steinbock, O. Chemical gardens without silica: the formation of pure metal hydroxide tubes. *Chem. Commun.* **2015**, *51* (65), 12962−12965.

(27) Ohgushi, H.; Dohi, Y.; Tamai, S.; Tabata, S. Osteogenic differentiation of marrow stromal stem cells in porous hydroxyapatite ceramics. *J. Biomed. Mater. Res.* **1993**, *27*, 1401−1407.

(28) Lovett, M.; Lee, K.; Edwards, A.; Kaplan, D. L. Vascularization Strategies for Tissue Engineering. *Tissue Eng., Part B* **2009**, *15*, 353−370.

(29) Nguyen, L. H.; Annabi, N.; Nikkah, M.; Bae, H.; Binan, L.; Park, S.; Kang, Y.; Yang, Y.; Khademhosseini, A. Vascularized Bone Tissue Engineering: Approaches for Potential Improvement. *Tissue Eng., Part B* **2012**, *18*, 363−382.

(30) Hwang, K. J.; Hwang, C. H.; Lee, I. H.; Kim, T.; Jin, S.; Park, J. Y. Synthesis and characterization of hollow metal oxide micro-tubes using a biomaterial template. *Biomass Bioenergy* **2014**, *68*, 62−66.

(31) Iruela-Arispe, M. L.; Beitel, G. J. Tubulogenesis. *Development* **2013**, *140*, 2851−2855.

(32) Raghavan, S.; Nelson, C. M.; Baranski, J. D.; Lim, E.; Chen, C. S. Geometrically Controlled Endothelial Tubulogenesis in Micropatterned Gels. *Tissue Eng., Part A* **2010**, *16*, 2255−2263.

(33) Punia, K.; Bucaro, M.; Mancuso, A.; Cuttitta, C.; Marsillo, A.; Bykov, A.; L'Amoreaux, W.; Raja, K. S. Rediscovering Chemical Gardens: Self-Assembling Cytocompatible Protein-Intercalated Silicate-Phosphate Sponge-Mimetic Tubules. *Langmuir* **2016**, *32* (34), 8748−58.

(34) Makki, R.; Al-Humiari, M.; Dutta, S.; Steinbock, O. Hollow Microtubes and Shells from Reactant-Loaded Polymer Beads. *Angew. Chem., Int. Ed.* **2009**, *48* (46), 8752−8756.

(35) Thouvenel-Romans, S.; Pagano, J. J.; Steinbock, O. Bubble guidance of tubular growth in reaction-precipitation systems. *Phys. Chem. Chem. Phys.* **2005**, *7* (13), 2610−2615.

(36) Deutsch, W. J. *Groundwater Geochemistry: Fundamentals and Applications to Contamination*; CRC Press, 1997.

(37) Jowsey, J. Studies of Haversian systems in man and some animals. *J. Anat.* **1966**, *100*, 857−864.

(38) Cooper, D. M.; Thomas, C. D.; Clement, J. G.; Turinsky, A. L.; Sensen, C. W.; Hallgrimsson, B. Age-dependent change in the 3D structure of cortical porosity at the human femoral midshaft. *Bone.* **2007**, *40*, 957−965.

(39) Addadi, L.; Weiner, S. Control and Design Principles in Biological Mineralization. *Angew. Chem., Int. Ed. Engl.* **1992**, *31*, 153−169.

DOI: 10.1021/acs.langmuir.6b04574
Langmuir 2017, 33, 2059−2067

(40) Batista, B. C.; Cruz, P.; Steinbock, O. Self-Alignment of Beads and Cell Trapping in Precipitate Tubes. *ChemPhysChem* **2015**, *16* (11), 2299−2303.

DOI: 10.1021/acs.langmuir.6b04574
Langmuir 2017, 33, 2059−2067